Atmos. Meas. Tech. Discuss., 5, 8405–8434, 2012
www.atmos-meas-tech-discuss.net/5/8405/2012/
doi:10.5194/amtd-5-8405-2012
© Author(s) 2012. CC Attribution 3.0 License.

Atmospheric Measurement Techniques Discussions

This discussion paper is/has been under review for the journal Atmospheric Measurement Techniques (AMT). Please refer to the corresponding final paper in AMT if available.

Assessment of COSMIC radio occultation retrieval product using global radiosonde data

B.-R. Wang[1,2], **X.-Y. Liu**[1], **and J.-K. Wang**[1]

[1]Dept. of Atmospheric and Oceanic Sciences, School of Physics, Peking University, Beijing, China
[2]Aviation Meteorological Center, Air Traffic Management Bureau, Civil Aviation Administration of China, Beijing, China

Received: 12 October 2012 – Accepted: 4 November 2012 – Published: 23 November 2012

Correspondence to: B.-R. Wang (markwangpk@gmail.com)

Published by Copernicus Publications on behalf of the European Geosciences Union.

Abstract

The radio occultation retrieval product of the Constellation Observing System for Meteorology, Ionosphere, and Climate (COSMIC) radio occultation sounding system was verified using the global radiosonde from 2007 to 2010. 4 yr of samples were used to collect quantities of data using much stricter matching criteria than previous studies to obtain more accurate results. The horizontal distance between the radiosonde station and the occultation event is within 100 km, and the time window is 1 h. The comparison was performed from 925 hPa to 10 hPa. The results indicated that the COSMIC's temperature data agreed well with the radiosonde data. The global mean temperature bias was −0.09 K, with a standard deviation (SD) of 1.72 K. The water vapor pressure of COSMIC showed a systematic bias in relation to radiosonde in higher layers. The mean specific humidity bias of 925–200 hPa is about $-0.011\,g\,kg^{-1}$, with a SD of about $0.662\,g\,kg^{-1}$. The COSMIC quality control process could not detect some abnormal extremely small humidity data which occured frequently in subtropical zone. Despite the large relative error of water vapor pressure, the relative error of refractivity is small. This paper also provides a comparison of eight radiosonde types with COSMIC product. Because the retrieval product is affected by the background error which differed between different regions, the COSMIC retrieval product could be used as a benchmark if the precision requirement is not strict.

1 Introduction

COSMIC (Constellation Observation System for Meteorology Ionosphere and Climate) is a GPS (Global Positioning System) radio occultation observation system. It consists of six identical microsatellites, and was launched successfully on 14 April 2006. GPS radio occultation observation has the advantage of near-global cover, all-weather capability, high vertical resolution, high accuracy and self-calibration (Yunch et al., 2000; Steiner et al., 1999; Hajj et al., 2000; Kursinski et al., 2000).

AMTD
5, 8405–8434, 2012

The conventional method of observing high vertical resolution atmospheric pressure, temperature and humidity profiles is radiosonde sounding. It's a practical way to verify the COSMIC product data quality using radiosonde data. Assessment of GPS/MET indicated that radio occultation sounding provides good temperature accuracy, with bias of about 1 K from the lower troposphere to 40 km (Ware et al., 1996; Kursinski et al., 1996; Rocken et al., 1997). The studies in CHAMP (CHAllenging Minisatellite Payload) substantiated the results of GPS/MET, finding that radio occultation sounding has high accuracy from about 5 km to 25 km (Hajj et al., 2004; Kuo et al., 2004, 2005). Fu et al. (2009) assessed the COSMIC results using Australian radiosonde station data for a 13-month period. Sun et al. (2010) performed a comparison for 18 months. He et al. (2009) compared the temperatures in the upper troposphere and lower stratosphere using radiosonde data. Ho et al. (2010) compared the specific humidity profile with radiosonde and ECMWF (European Centre for Medium-Range Weather Forecasts) analysis for 4 months. Kishore et al. (2008) validated the first year of COSMIC observation. These studies indicated that the results of COSMIC show good agreement with radiosonde, especially the temperature data (see in Table 1). However, the collocation mismatch criteria were not strict due to the short data periods in those studies, or the comparisons were performed over restricted regions. Sun et al. (2010) reported that, in the troposphere (850–200 hPa), the collocation mismatch impacts on the comparison standard deviation errors for temperature are 0.35 K/3 h and 0.42 K/100 km and for relative humidity are 3.3 %/3 h and 3.1 %/100 km. In the present study, the assessment used 4 yr of data from 2007 to 2010. A longer period was used to collect sufficient samples to reduce the collocation mismatch. This comparison used the 1DVAR retrieval product wetPrf. The background used for 1DVAR process is the ECMWF analysis data, which was recorded in ecmPrf data.

However, radiosonde itself suffers from measurement bias, such as radiation errors in temperature measurements and various errors in humidity (Luers et al., 1998; Wang et al., 2003, 2008; Miloshevich et al., 2006). In addition to the sensor limitation, the radiosonde bias differs among stations due to geographical distribution and differences

AMTD
5, 8405–8434, 2012

in radiosonde type (Soden et al., 1996; Christy et al., 2009). Besides the measurement error, the comparison also included representativeness error. Radiosonde sounding is a point measurement, whereas radio occultation sounding actually measures the averages over finite volumes of the atmosphere (Kuo et al., 2004). Horizontal drift exists in both COSMIC and radiosonde profiles. Radiosonde balloon would drift because of the horizontal wind. Seidel et al. (2011) studied the global radiosonde balloon drift of 419 stations for the 2 yr period from July 2007 to June 2009. The results indicated mean drift distances of < 20 km in the upper troposphere, and < 50 km in the lower stratosphere.

As the COSMIC data have global coverage and are stable, although the 1DVAR retrieval product contains the information of background, it could be used as a benchmark to evaluate the other observation data or model analysis (Sun et al., 2010; He et al., 2009; Ho et al., 2010). In this study, eight radiosonde types were chosen for the comparison to verify the relative accuracy between the COSMIC product and different radiosonde types. As the COSMIC product is also affected by the background error we will discuss whether it is suitable for use as a benchmark.

2 Data and comparison method

The COSMIC 1DVAR retrieval product wetPrf profiles and global radiosonde profiles from 2007 to 2010 were used for this comparison. The wetPrf profiles were downloaded from COSMIC Data Analysis and Archive Center (CDAAC). The data version was 2010.2640. The wetPrf data altitude range is 0–40 km at 100 m vertical resolution, and it included the parameters of atmospheric pressure, geometric height, temperature, water vapor pressure, etc. These data provided more than 1700 profiles globally per day on average from 2007 to 2010. The radiosonde profiles were downloaded from the Integrated Global Radiosonde Archive (IGRA) which includes radiosonde and pilot balloon observations from over 1500 globally distributed stations.

AMTD
5, 8405–8434, 2012

The statistics of the COSMIC data from 2007 to 2010 indicated that the mean target point horizontal drift distance from altitude 1 km to 10 km was about 102 km, and the drift distance from 1 km to 20 km was about 136 km. In this study, the horizontal mismatch distance limit between the COSMIC occultation tangent point at the height of 10 km and the radiosonde station was set to 0.9° in central angle difference whicha is a horizontal distance of about 100 km. The radiosonde data of UTC 00:00 and 12:00 were used, and the time window was 1 h. A total of 737 radiosonde stations, whose distribution is shown in Fig. 1, were matched in this comparison. Eight kind of radiosonde types were selected for comparison between different radiosonde types with COSMIC products. The stations using these radiosonde types are shown in different colors in Fig. 1.

The wetPrf profile altitude range was 0–40 km with high vertical resolution of 100 m. However, the downloaded radiosonde data had a much lower vertical resolution. To avoid errors from due to interpolation of radiosonde profiles, the comparison was performed only on the standard pressure levels of the radiosonde profile. The standard pressure levels were from 1000 hPa to 5 hPa, with a total of 18 layers. The numbers of radiosonde data in 7 hPa and 5 hPa layers were small, and there were also insufficient wetPrf data at the 1000 hPa layer. Therefore, the comparison was performed at 15 pressure levels from 925 hPa to 10 hPa. The water vapor pressure of radiosonde data is given by Goff–Gratch equation (Murphy et al., 2005). The atmospheric refractivity of radiosonde is calculated using this function:

$$N = 77.6\frac{P}{T} + 3.73 \times 10^5 \frac{\mathrm{Vp}}{T^2}, \quad (1)$$

where N is refractivity, T is temperature in Kelvin, and P and Vp are total air pressure and partial pressure of water vapor at hPa, respectively.

AMTD
5, 8405–8434, 2012

The wetPrf data is recorded in altitude layers. It needs to be interpolated into pressure layers. The interpolation of wetPrf data is performed as:

$$\alpha = \frac{\ln P - \ln P_2}{\ln P_1 - \ln P_2}, \beta = \frac{\ln P_1 - \ln P}{\ln P_1 - \ln P_2}, \quad (2)$$

$$T = \alpha \cdot T_1 + \beta \cdot T_2, \quad (3)$$

$$q = \alpha \cdot q_1 + \beta \cdot q_2, \quad (4)$$

$$\mathrm{Vp} = \exp[\alpha \cdot \ln(\mathrm{Vp}_1) + \beta \cdot \ln(\mathrm{Vp}_2)], \quad (5)$$

$$N = \alpha \cdot N_1 + \beta \cdot N_2 \quad (6)$$

where P is the pressure of the standard pressure level, subscript 1 and 2 stands for the parameters from wetPrf.

The interpolation is performed in a manner similar to linear interpolation of altitude. As the wetPrf data have high vertical resolution, the difference between different interpolation methods is small.

The comparison was performed in terms of temperature difference ΔT, specific humidity difference Δq, relative error of water vapor pressure RE Vp and relative error of refractivity RE N, which are given by Eqs. (7) to (10), respectivity.

$$\Delta T = T_{\mathrm{wetPrf}} - T_{\mathrm{radiosonde}}, \quad (7)$$

$$\Delta q = q_{\mathrm{wetPrf}} - q_{\mathrm{radiosonde}}, \quad (8)$$

$$\mathrm{RE\ Vp} = (\mathrm{Vp}_{\mathrm{wetPrf}} - \mathrm{Vp}_{\mathrm{radiosonde}})/\mathrm{Vp}_{\mathrm{radiosonde}}, \quad (9)$$

$$\mathrm{RE}\ N = (N_{\mathrm{wetPrf}} - N_{\mathrm{radiosonde}})/N_{\mathrm{radiosonde}}. \quad (10)$$

If RE Vp > +900 % or RE Vp < −90 %, the difference in the water vapor pressure of wetPrf and radiosonde is greater than one order of magnitude. We used specific humidity for comparison of absolute deviation and water vapor pressure for comparison of relative error because although the specific humidity has been used much more frequently in other studies, it includes the error of atmospheric pressure, so the relative error comparison just uses the water vapor pressure itself.

AMTD
5, 8405–8434, 2012

3 Comparison results

3.1 Bias and relative error distribution

A total of 7299 profiles matched globally from 2007 to 2010, including 93 511 radiosonde temperature data and 79 403 dew-point depression data. On average, a single profile included about 13 layers with temperature data and 11 layers with humidity data.

The left graphs in Fig. 2 show the mean temperature bias at each layer and their SDs. The mean temperature bias were all within ±0.5 K in each layer. The global mean temperature bias of 925–10 hPa was −0.09 K, with the SD of 1.72 K. The wetPrf temperature was a bit higher than the radiosonde temperature in the layers below 700 hPa (pressure larger than 700 hPa), and a bit lower in the layers above 700 hPa. The SD in the layers from 700 hPa to 150 hPa was within the range of 1.4–1.5 K; the SD increased in the higher layers above 100 hPa, with values of 2.07 K in the layer at 20 hPa increaseing rapidly to 2.90 K in the layer at 10 hPa. A large SD was also seen in the layers below 700 hPa, with a value of 2.21 K in the layer at 925 hPa.

The wetPrf water vapor pressure was much smaller compared to radiosonde in the layers above 200 hPa. Figure 3 shows the mean water vapor pressure profile of wetPrf, background and radiosonde. The wetPrf water vapor pressure was much more stable in the layers above 200 hPa, compared with radiosonde data. The radiosonde mean water vapor pressure showed no significant decrease in the layers above 200 hPa, which did not seem to be correct. Therefore, the comparison of humidity was focused in the layers below 200 hPa. Due to extreme relative error of the water vapor pressure which markedly affects the results, these data are removed from the comparison. Setting the limit of the relative error of water vapor pressure at −99 % to +9900 % (two orders of magnitude difference), in the layers of 925–200 hPa, 74 data are removed from the total of 49 772, leaving 49 698 data. Setting the limit of the relative error of water vapor pressure at −90 % to +900 % (one order of magnitude difference), 48 378

AMTD
5, 8405–8434, 2012

data remained, and 1394 data were removed. The comparison of specific humidity and water vapor pressure used the same samples.

The middle graphs in Fig. 2 show the mean absolute deviation of specific humidity and their SDs. The global mean specific humidity bias at 925–200 hPa was $-0.011\,g\,kg^{-1}$ ($-0.007\,g\,kg^{-1}$) with the relative error limit of water vapor pressure −90 % to +900 % (−99 % to +9900 %), and the SD was $0.662\,g\,kg^{-1}$ ($0.664\,g\,kg^{-1}$). The wetPrf specific humidity was smaller than radiosonde in near-ground layers, but the background humidity was larger. The wetPrf specific humidity bias and background bias were almost the same in the layers above 200 hPa. The wetPrf specific humidity was smaller than radiosonde in most layers, but was larger around the layer of 300 hPa. The right graphs in Fig. 2 show the mean relative error of water vapor pressure and their SDs. With the limit of −90 % to +900 % (−99 % to +9900 %), the mean relative error in the layers of 925–200 hPa was +34.0 % (+55.3 %), and the SD was 114.7 % (272.7 %), respectively. The layers around 300 hPa were more sensitive to the changes in relative error limit. Despite the large mean relative error, the mean absolute deviation was small.

The large mean relative error had relations with the distribution of the relative error and the function wich calculates the relative error. The negative relative error could only reach −100 %, but the positive relative error could be much larger than +100 %. Figure 4 shows the probability density of the relative error of water vapor pressure in the layers of 925–200 hPa. Although the peak is located on the negative side, the large positive relative error is greater than the negative error, and the mean relative error is positive. As shown in the figure, the limit of −90 % to +900 % is representative.

Figure 5 shows the distribution of the relative error of water vapor pressure in the layers of 925–200 hPa. Similar to the results shown in Fig. 4, the peak is located on the negative side, but the large positive relative error is greater than the negative error. The relative error is much larger if the water vapor pressure value is lower, especially when the radiosonde water vapor pressure value is lower than 0.1 hPa. Taking into consideration the data for which the radiosonde water vapor pressure is larger than

AMTD
5, 8405–8434, 2012

0.01 hPa/0.1 hPa, the mean relative error of water vapor pressure in the layers of 925–200 hPa is +27.2 %/+12.5 % with a relative error limit of −99 % to +9900 %. Considering all of the data without any radiosonde water vapor pressure limit, the value is +55.3 %.

Despite the the large relative error of water vapor pressure, the refractivity did not change markedly. Figure 8 shows the relative error of the refractivity from radio occultation observation, the 1DVAR product wetPrf, the background ecmPrf and the refractivity calculated from radiosonde, respectively. The large relative error of water vapor pressure had little effect on refractivity bias. The relative error of refractivity was within ±1.6 %. Noticeable differences between observation and retrieval product were seen only in the layers below 700 hPa. The differences of refractivity between radio occultation observation and the background were also larger in this region. The retrieval process would reduce the mean bias and SD in these layers.

3.2 Distribution of extreme relative error of water vapor pressure

Figure 6 shows the distribution of extreme relative error of water vapor pressure. The total number of matched water vapor data is 79 403, of which five and 654 had positive relative error larger than +9900 % and +900 %, respectively. All of these data are located at layers below 50 hPa, and the peak is located in the layer at 300 hPa. There are mainly three kinds of cases. In the frist case the value of radiosonde water vapor pressure is extremely low in the layer but normal in nearby layers. Usually, this low radiosonde water vapor pressure occurs in a single layer, so there would be a large positive relative error in this layer but normal in the layers nearby. The radiosonde water vapor pressure on the layer below could be 1000 % higher than the value in these layers, and the value in the layer above could be 200 % higher. Among the total of 79 403 data, 186 agreed this rule; only 20 of them whose relative error were less than 100 %. 63 of them had positive relative error larger than +900 %, representing only about 10 % of all the extreme positive relative bias data. The peak is located at 500 hPa which is also different from the peak at 300 hPa considering all the data. Therefore, the first case

AMTD
5, 8405–8434, 2012

would not include a large number of data. In the second case radiosonde profile had much larger water vapor pressure decrease rate than wetPrf. Although wetPrf's mean water vapor pressure was larger than radiosonde in lower layers and smaller in higher layers, which means that wetPrf had a larger mean decrease rate than radiosonde, the water vapor pressure of radiosonde sometimes decreased much faster or began to decrease rapidly in lower layers compared with wetPrf. Usually, the second case occured in the layer of 500–200 hPa. The peak was located at 300 hPa, which was also the peak of positive absolute deviation and relative error. Most data with extreme positive relative error of water vapor pressure belonged to the second case. In the third case wetPrf's water vapor pressure was systematic larger than radiosonde. Usually, this case occured in the layer blow 500 hPa. The number of the third case was small compared to the second case.

1786 out of the total 79 403 data had negative relative error larger than −99 % and 14 308 were larger than −90 %. Most occured in the layers above 200 hPa, due to the systematic humidity bias in these layers. The number of extreme negative relative errors was much smaller compared with the extreme positive ones in the layers below 200 hPa. Most of extreme negative relative error in lower layers belonged to this case, in which the value of wetPrf water vapor pressure was extremely low in the layer but normal in lower and higher layers. The extremely low water vapor pressure seemed to be not consistent with the real atmosphere (e.g. in the profile of C003.2008.287.11.55, the water vapor pressure was 1×10^{-6} hPa at the height of 5.7–6.3 km), and the quality control process did not eliminate these data. A single profile could have more than one layer of the extremely low water vapor pressure. About 7.6 % of the wetPrf profiles included at least one layer of extremely low water vapor pressure, the mean total thickness of the extremely low water vapor pressure layer in a single profile was about 414 m. The majority of this phenomenon occured in layers below 10 km, especially in the altitude region of 2–8 km, but it also occured in layers above 10 km. Figure 8 shows the distribution of the probability of the profile which included extremely low water vapor pressure (less than 2×10^{-6} hPa). Most of the extremely low water vapor pressure

AMTD
5, 8405–8434, 2012

occured below 10 km were located in the latitude region of −45°–45°, especially in subtropical zone, and most of the extremely low water vapor pressure occured above 10 km were located in the latitude region of −90° to −45° and 45°–90° . This phenomenon was often concomitant with smaller observed refractivity, smaller retrieved refractivity and higher retrieved temperature than those of background. If the observed refractivity was much smaller than background, the 1DVAR process trended to generate smaller water vapor pressure and higher temperature. If the refractivity bias was large enough, the retrieved water vapor pressure might be extremely small or even negative. But things were different in near-ground layers, statistics indicated that the extremely low water vapor pressure phenomenon could be concomitant with larger observed and retrieved refractivity than background when altitude was less than 1 km, and lower temperature than background when altitude was less than 2 km. Overall, the large value regions in Fig. 8 indicated that large negative refractivity bias in COSMIC observation and background ECMWF analysis occured frequently in those regions.

We had developed a 1DVAR retrieval algorithm which generate temperature and specific humidity profiles using COSMIC's refractivity profile and ECMWF analysis. The results showed that the error covariance matrixes have significant influence on the retrieval profiles. The extremely small water vapor pressure could be abated if the the error covariance matrixes were adjusted properly. However, this would make the retrieved water vapor pressure profile closer to the background, and the temperature profile was also affected.

3.3 Comparison of the results with different radiosonde types

COSMIC provides global coverage of radio occultation observations and can be used to assess other observations or model results (Sun et al., 2010; He et al., 2009; Ho et al., 2010). Here we present a comparison of COSMIC proudt with eight different radiosonde types. As many of the radiosonde types are used in limited regions, this comparison can be used to determine the bias of COSMIC in these regions if we use radiosonde data as benchmarks. The radiosonde types included in the comparison

AMTD
5, 8405–8434, 2012

were GTS1 and GZZ-2 (China), MEISEI (Japan), MRZ-3A (Russia), two types of VIZ (USA), and VAISALA RS80 and RS92. However, there was a problem in that the wetPrf product is produced through a 1DVAR retrieval process using the ECMWF analysis as the background, and it is therefore affected by the different background errors in different regions. Therefore, the comparison is more likely to indicate how the wetPrf data match those from certain types of radiosonde in certain regions. In this comparison, the radiosonde data were set as the benchmarks. It was assumed that the error of a certain kind of radiosonde type will remain the same in different regions. The method used was the same as that in the comparisons described above (Eqs. 7–9). An inverse process is needed to determine the differences among different radiosonde types. For example, a lower curve in mean temperature bias figure indicates that the radiosonde type will yield higher temperature data compared with the other types.

The comparison results are showed in Fig. 9 and the mean bias results are showed in Table 2. The left graphs in Fig. 9 show the results of temperature comparison. Most of these radiosonde types showed similar performance. However, MRZ-3A was unique, in that it had much higher temperature compared with the other radiosonde types, especially at layers around 300 hPa. Conversely, VIZ/SIPPICAN MICROSONDE MKIIA GPS had lower temperature than others. These results indicated that the temperatures of the two radiosonde types used in China were slightly higher than those of the other radiosonde types. GTS1 showed better performance than GZZ-2, and GZZ-2 had much higher SD at higher layers than the other types if the error of COSMIC product remained the same in different regions.

The middle graphs in Fig. 9 show the absolute deviation of specific humidity in layers from 925 hPa to 200 hPa. MRZ-3A and JAPAN MEISEI RSII-91RH CORRECTION had larger value compared to the other types. In the layers below 850 hPa, VIZ/SIPPICAN MICROSONDE MKIIA GPS had the largest positive bias, but in other layers its bias was small. The two radiosonde types used in China had much smaller specific humidity in layers below 500 hPa. The right graphs in Fig. 9 show the relative error of water vapor pressure in layers from 925 hPa to 200 hPa. MRZ-3A was still unique, it had negative

AMTD
5, 8405–8434, 2012

mean relative error while the others had positive mean relative error. GZZ-2 showed similar performance to the others. However, GTS1 still had much lower water vapor pressure values than the others, and its SD was the largest.

3.4 Influence of background data

wetPrf is the COSMIC 1DVAR retrieval product which uses the ECMWF analysis as the background, and it is therefore affected by the background. Figure 10 shows the relative error between observed, background and retrieved refractivity and the refractivity calculated from radiosonde, respectively. The same comparison method as that in the comparisons described above was used, the radiosonde was set as the benchmark (Eq. 10). The observed refractivity of COSMIC in the region of China was normal or slightly smaller than in the others in the layers below 500 hPa, and so did the SD. After the retrieval process, the SDs of these two radiosonde types became normal compared with the others, but the mean refractivity became much smaller than the other types. This phenomenon may have been due to the background error if the retrieval algorithm was stable globally. The refractivity data of background ecmPrf in China had much larger bias from radiosonde than in the other regions, and the refractivity in this region was much smaller than that in the other regions. As shown in the figure, the retrieved refractivity was much more similar to the background than to the observation. The error of wetPrf data was affected by the background error, and the background error showed considerable differences between different regions. The figure of the relative error of refractivity is similar to the figure of the specific humidity bias in Sect. 3.3.

Although some studies have indicated that COSMIC is suitable as a benchmark (Sun et al., 2010; He et al., 2009; Ho et al., 2010), we feel that the retrieval product could be used as benchmark if no better method is available, or if the precision requirement is not particularly strict, or if the background error is well known. As the refractivity observation is not affected by background, the observed refractivity profile is more suitable to be used as a benchmark than the 1DVAR retrieval product. There were

AMTD
5, 8405–8434, 2012

noticeable differences between different versions of the wetPrf data, and improvement of the retrieval process may reduce the bias.

4 Conclusions

As the collocation mismatch has an impact on the comparison standard deviations (Sun et al., 2010), we collected samples for the four years from 2007 to 2010 to obtain sufficient data with stricter matching rules used than in previous studies so as to obtain more accurate results. The matching criteria were 1 h and 100 km. The COSMIC 1DVAR product wetPrf showed good atmospheric temperature data quality. The global mean temperature bias at 925–10 hPa was −0.09 K, with a standard deviation of 1.72 K. The wetPrf temperature was slightly higher than radiosonde below the layer of 700 hPa and was slightly lower above. The radiosonde humidity was significantly larger than wetPrf and background ecmPrf above the layer of 200 hPa. As the radiosonde humidity data was not reliable above the layer of 200 hPa, the comparison of humidity was focused in the layers below 200 hPa. The global mean specific humidity bias at 925–200 hPa was about $-0.011\,g\,kg^{-1}$, with a standard deviation of about $0.662\,g\,kg^{-1}$. The mean absolute deviation of specific humidity was small, but the relative error was significantly large. The mean relative error of water vapor pressure in the pressure range of 925–200 hPa was about +34 % to +55 %, depending on the different data filtration used in this paper. The peak of positive relative error was located at about 300 hPa. The large relative error might have been due to the extremely small humidity data of radiosonde or wetPrf, or to the differences in the rate of decrease in humidity. The quality control process of COSMIC did not detect some abnormal extremely small humidity data. The majority of this phenomenon occured in subtropical zone. The extremely small humidity data was generated by 1DVAR process when the observed refractivity was significantly smaller than background. The large relative error of water vapor pressure had little effect on refractivity. The 1DVAR retrieval process would reduce the

AMTD
5, 8405–8434, 2012

refractivity bias and the standard deviation in near-ground layers. The differences between retrieved refractivity and observation were small on layers above 200 hPa.

Comparison of COSMIC with different radiosonde types demonstrated its ability to assess other observation data. All of the eight radiosonde types showed good temperature agreement with wetPrf. The performance of MRZ-3A from Russia was unique, which was probably due to the high latitude region in which the radiosonde equipment is located. The two Chinese radiosonde types performed well. However, the humidity of the two Chinese radiosonde types were significantly smaller compared with the other types. One possible reason for this is the ECMWF analysis data which was used as the background. The refractivity bias in the region of China between ECMWF analysis and radiosonde were much larger than the other regions, similar to the results of the humidity comparison between wetPrf and radiosonde. The retrieved refractivity was much more similar to the background than to the observation in near-ground layers, and the retrieved refractivity was much closer to the observation in higher layers. The COSMIC product wetPrf could be used as a benchmark if the precision requirement is not strict, or if no better alternative is available, or the background error is well known. Another problem is that the COSMIC data coverage is still insufficient, an improvement must await the launch of COSMIC II.

Acknowledgements. The authors are grateful to the COSMIC Data Analysis and Archive Center (CDAAC) and Integrated Global Radiosonde Archive (IGRA) for providing their data. This work was funded by the National Natural Science Foundation of China (41075011) and Special Fund for Meteorology Research in the Public Interest (GYHY201006037).

AMTD
5, 8405–8434, 2012

References

Christy, J. R. and Norris, W. B.: Discontinuity issues with radiosonde and satellite temperatures in the Australian region 1979–2006, J. Atmos. Ocean. Tech., 26, 508–522, doi:10.1175/2008JTECHA1126.1, 2009.

Fu, E.-J., Zhang, K.-F., Ka-yea, M., Xu, X.-H., John, M., Anthony, R., Gary, W., and Yuriy, K.: Assessing COSMIC GPS radio occultation derived atmospheric parameters using Australian radiosonde network data, Procedia Earth and Planetary Science, 1, 1054–1059, 2009.

Hajj, G. A., Lee, L. C., Pi, X., Romans, L. J., Schreiner, W. S., Straus, P. R., and Wang, C.: COSMIC GPS ionospheric sensing and space weather, Terr. Atmos. Ocean. Sci., 11, 235–272, 2000.

Hajj, G. A., Ao, C. O., Iijima, B. A., Kuang, D., Kursinski, E. R., Mannucci, A. J., Meehan, T. K., Romans, L. J., de la Torre Juarez, M., and Yunck, T. P.: CHAMP and SAC-C atmospheric results and intercomparisons, J. Geophys. Res., 109, D06109, doi:10.1029/2003JD003909, 2004.

He, W., Ho, S.-P., Chen, H., Zhou, X., Hunt, D., and Kuo, Y.-H.: Assessment of radiosonde temperature measurements in the upper troposphere and lower stratosphere using COSMIC radio occultation data, Geophys. Res. Lett., 36, L17807, doi:10.1029/2009GL038712, 2009.

Ho, S.-P., Zhou, X., Kuo, Y.-H., Hunt, D., and Wang, J.-H.: Global evaluation of radiosonde water vapor wystematic biases using GPS radio occultation from COSMIC and ECMWF analysis, Remote Sens., 2, 1320–1330, doi:10.3390/rs2051320, 2010.

Kishore, P., Namboothiri, S. P., Jiang, J. H., Sivakumar, V., and Igarashi, K.: Global temperature estimates in the troposphere and stratosphere: a validation study of COSMIC/FORMOSAT-3 measurements, Atmos. Chem. Phys., 9, 897–908, doi:10.5194/acp-9-897-2009, 2009.

Kuo, Y.-H., Wee, T.-K., Sokolovskiy, S., Rocken, C., Schreiner, W., Hunt, D., and Anthes, R. A.: Inversion and error estimation of GPS radio occultation data, J. Meteorol. Soc. Jpn., 82, 507–531, doi:10.2151/jmsj.2004.507, 2004.

Kuo, Y.-H., Schreiner, W. S., Wang, J., Rossiter, D. L., and Zhang, Y.: Comparison of GPS radio occultation soundings with radiosondes, Geophys. Res. Lett., 32, L05817, doi:10.1029/2004GL021443, 2005.

Kursinski, E. R., Hajj, G. A., Bertiger, W. I., Leroy, S. S., Meehan, T. K., Romans, L. J., Schofield, J. T., Mccleese, D. J., Melbourne, W. G., Thornton, C. L., Yunck, T. P., Eyre, J. R., and Nagatani, R. N.: Initial results of radio occultation observations of

AMTD
5, 8405–8434, 2012

Earth's atmosphere using the Global Positioning System, Science, 271, 1107–1110, doi:10.1126/science.271.5252.1107, 1996.
Kursinski, E. R., Hajj, G. A., Leroy, S. S., and Herman, B.: The GPS radio occultation technique, Terr. Atmos. Ocean. Sci., 11, 53–114, 2000.
Luers, J. K. and Eskridge, R. E.: Use of radiosonde temperature data in climate studies, J. Climate, 11, 1002–1019, 1998.
Miloshevich, L. M., Vömel, H., Whiteman, D. N., Lesht, B. M., Schmidlin, F. J., and Russo, F.: Absolute accuracy of water vapor measurements from six operational radiosonde types launched during AWEXG and implications for AIRS validation, J. Geophys. Res., 111, D09S10, doi:10.1029/2005JD006083, 2006.
Murphy, D. M. and Koop, T.: Review of the vapour pressures of ice and supercooled water for atmospheric applications, Q. J. Roy. Meteorol. Soc., 131, 1539–1565, doi:10.1256/qj.04.94, 2005.
Rocken, C., Anthes, R., Exner, M., Hunt, D., Sokolovskiy, S., Ware, R., Gorbunov, M., Schreiner, W., Feng, D., Herman, B., Kuo, Y.-H., and Zou, X.: Analysis and validation of GPS/MET data in the neutral atmosphere, J. Geophys. Res., 102, 29849–29866, 1997.
Seidel, D. J., Sun, B., Pettey, M., and Reale, A.: Global radiosonde balloon drift statistics, J. Geophys. Res., 116, D07102, doi:10.1029/2010JD014891, 2011.
Steiner, A. K., Kirchengast, G., and Ladreiter, H. P.: Inversion, error analysis, and validation of GPS/MET occultation data, Ann. Geophys., 17, 122–138, doi:10.1007/s00585-999-0122-5, 1999.
Soden, B. J. and Lanzante, J. R.: An assessment of satellite and radiosonde climatologies of upper tropospheric water vapor, J. Climate, 9, 1235–1250, doi:10.1175/1520-0442(1996)009<1235:AAOSAR>2.0.CO;2, 1996.
Sun, B., Reale, A., Seidel, D. J., and Hunt, D. C.: Comparing radiosonde and COSMIC atmospheric profile data to quantify differences among radiosonde types and the effects of imperfect collocation on comparison statistics, J. Geophys. Res., 115, D23104, doi:10.1029/2010JD014457, 2010.
Wang, J. and Zhang, L.: Systematic errors in global radiosonde precipitable water data from comparisons with groundbased GPS measurements, J. Climate, 21, 2218–2238, doi:10.1175/2007JCLI1944.1, 2008.
Wang, J., Carlson, D. J., Parsons, D. B., Hock, T. F., Lauritsen, D., Cole, H. L. Beierle, K., and Chamberlain, E.: Performance of operational radiosonde humidity sensors in direct

AMTD
5, 8405–8434, 2012

comparison with a chilled mirror dew-point hygrometer and its climate implication, Geophys. Res. Lett., 30, 1860, doi:10.1029/2003GL016985, 2003.

Ware, R., Exner, M., Feng, D., Gorbunov, M., Hardy, K., Herman, B., Kuo, Y., Meehan, T., Melbourne, W., Rocken, C., Schreiner, W., Sokolovskiy, S., Solheim, F., Zou, X., Anthes, R., Businger, S., and Trenberth, K.: GPS sounding of the atmosphere from low earth orbit: preliminary results, B. Am. Meteorol. Soc., 77, 19–40, doi:10.1175/1520-0477(1996)077<0019:GSOTAF>2.0.CO;2, 1996.

Yunck, T. P., Liu, C., and Ware, R.: A history of GPS sounding, Terr. Atmos. Ocean. Sci., 11, 1–20, 2000.

AMTD
5, 8405–8434, 2012

Table 1. Results of the temperature bias between COSMIC and radiosonde.

Authors	Region	Period	Time window	Distance limit	Vertical range	ΔT	SD ΔT
Fu et al. (2009)	Australian	13 months	2 h	100 km	0–30 km	−0.43 K	1.53 K
Sun et al. (2010)	Global	19 months	6 h	250 km	850–200 hPa	< 0.15 K	1.5–2.0 K
He et al. (2009)	Global	9 months	2 h	300 km	12–25 km	< 0.5 K	< 2.0 K

AMTD
5, 8405–8434, 2012

Table 2. Mean bias of different radiosonde types between wetPrf and radiosonde*.

Type			925–200 hPa				
	ΔT (K)	SD ΔT (K)	Δq ($g\,kg^{-1}$)	SD Δq ($g\,kg^{-1}$)	RE Vp	SD RE Vp	Num. of profiles
CHINA GTS1 1680 MHZ	−0.070	1.670	0.079	0.693	78.8 %	171.0 %	553
CHINA GZZ-2 403 MHZ	−0.104	1.667	0.082	0.688	45.3 %	123.3 %	203
JAPAN MEISEI RSII-91 RH CORRECTION	0.003	1.583	−0.059	0.946	32.7 %	117.1 %	139
RUSSIA/USSR MRZ-3A	−0.330	1.757	−0.047	0.479	−11.0 %	52.9 %	1542
VIZ/SIPPICAN B2 1492-540 NWS 1680 MHZ	0.105	1.719	0.005	0.731	35.8 %	121.3 %	380
VIZ/SIPPICAN MICROSONDE MKIIA GPS	0.176	1.541	−0.017	0.716	58.4 %	144.7 %	613
VAISALA RS80	−0.002	1.560	−0.006	0.654	48.0 %	117.6 %	2288
VAISALA RS92	0.024	1.521	−0.020	0.666	62.1 %	127.5 %	343

* Equations (7)–(9) were used. The water vapor pressure relative error limit was −90 % to 900 %.

AMTD
5, 8405–8434, 2012

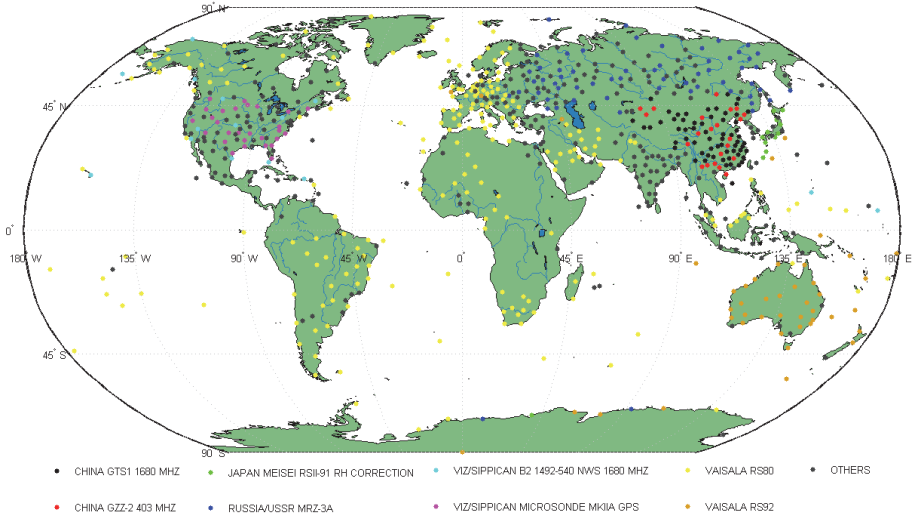

Fig. 1. Distributions of matched radiosonde stations.

AMTD
5, 8405–8434, 2012

COSMIC radio occultation retrieval product using global radiosonde data

B.-R. Wang et al.

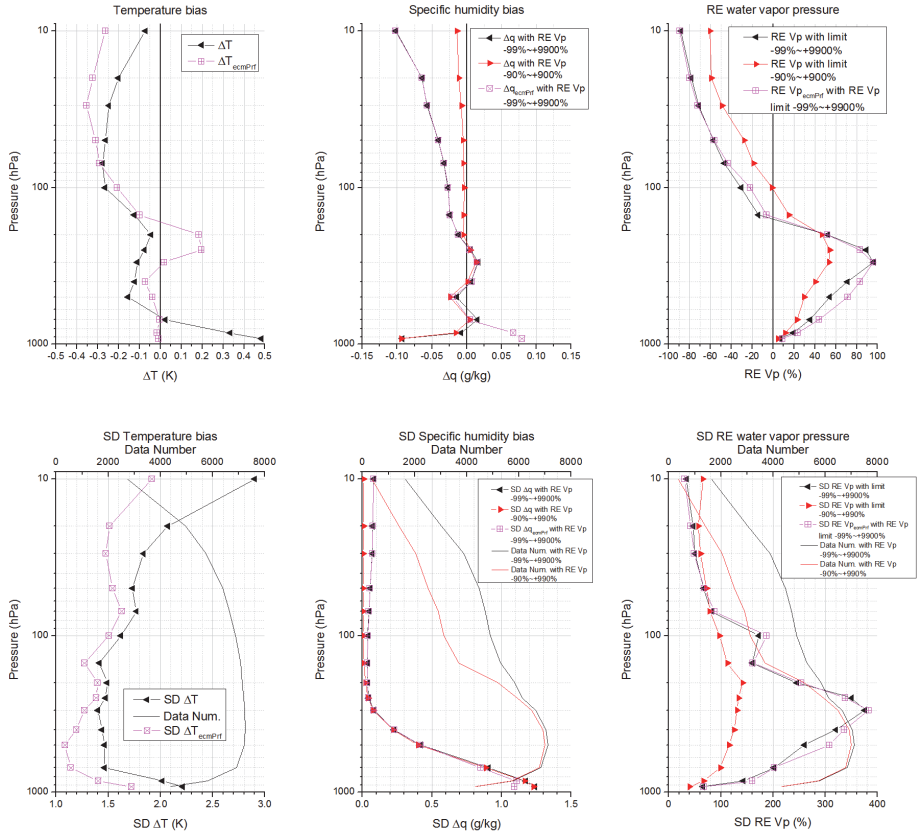

Fig. 2. Comparison of mean temperature bias, mean specific humidity bias, relative error of water vapor pressure and their SDs. The purple curves show the results of the background ecmPrf, curves without symbols show the data number.

AMTD
5, 8405–8434, 2012

COSMIC radio occultation retrieval product using global radiosonde data

B.-R. Wang et al.

CC BY

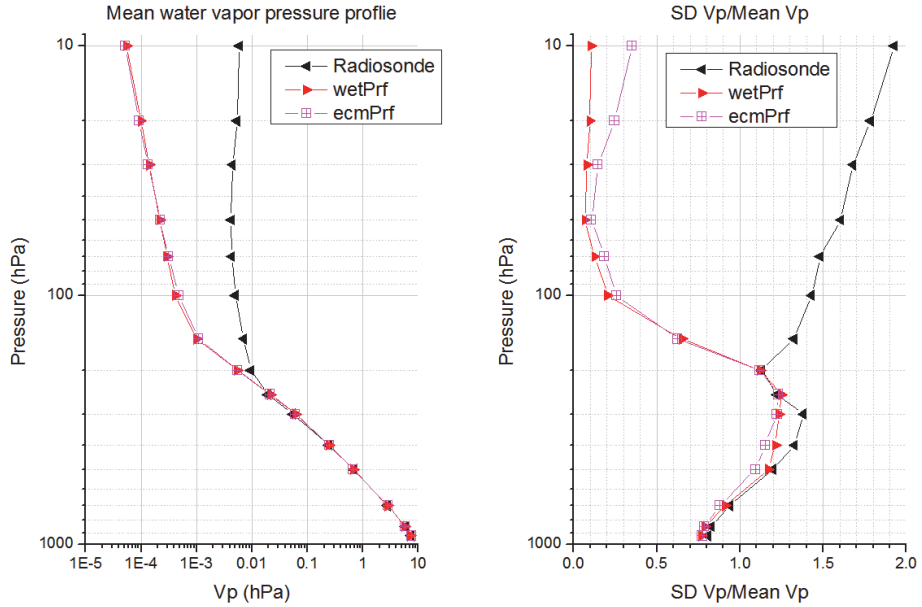

Fig. 3. Mean water vapor pressure profile of radiosonde, wetPrf and the background ecmPrf.

AMTD
5, 8405–8434, 2012

COSMIC radio occultation retrieval product using global radiosonde data

B.-R. Wang et al.

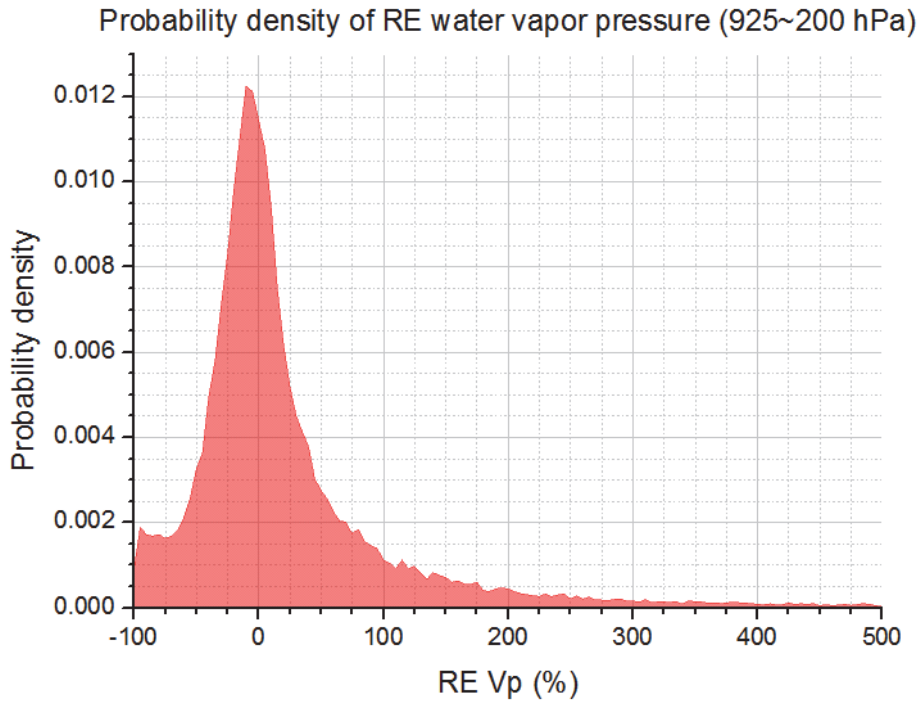

Fig. 4. Probability density of the relative error of water vapor pressure in the layers of 925 to 200 hPa.

AMTD
5, 8405–8434, 2012

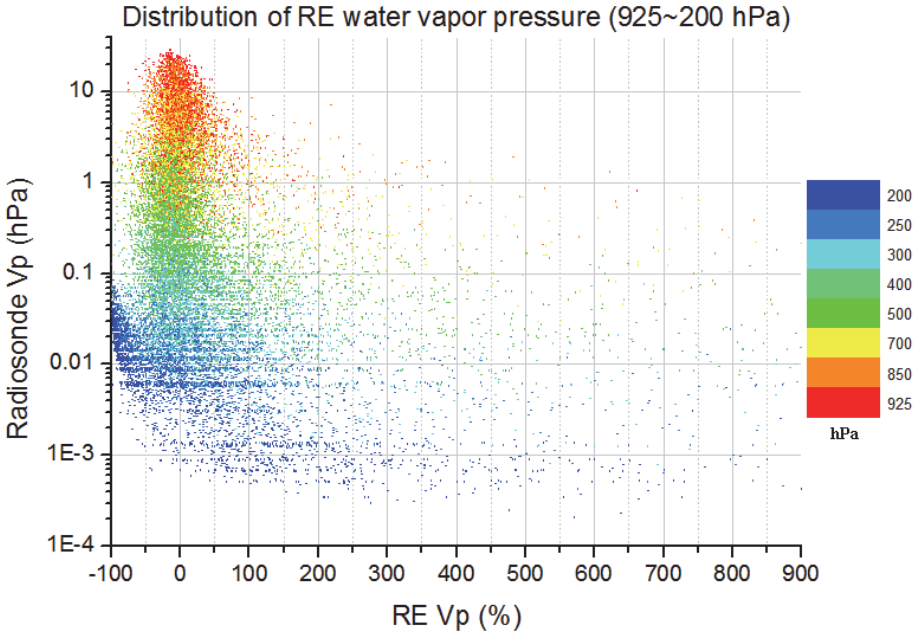

Fig. 5. Distribution of the relative error of water vapor pressure in the layers of 925 to 200 hPa.

AMTD
5, 8405–8434, 2012

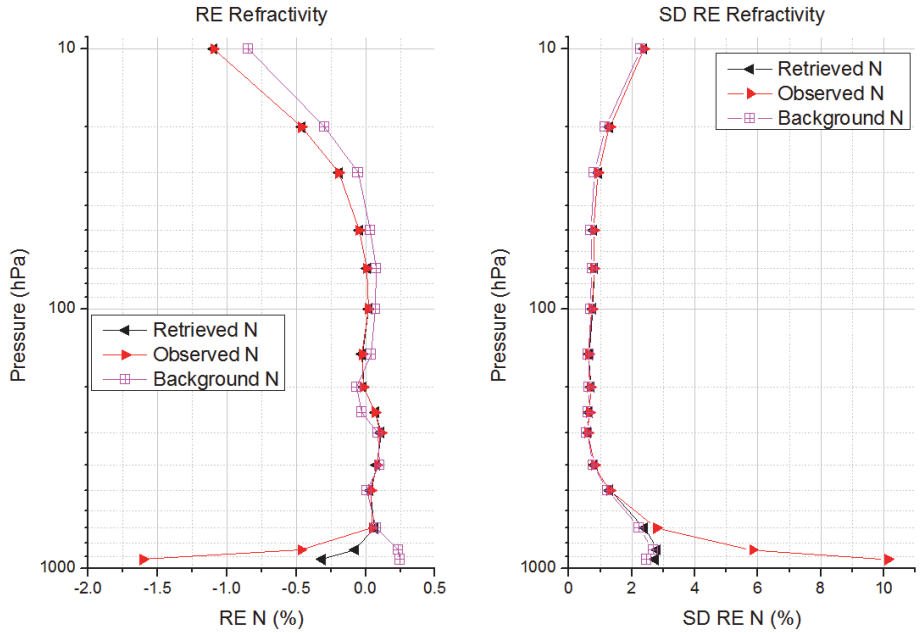

Fig. 6. Relative error and SD between the refractivity from the radio occultation observation, retrieval product wetPrf, background ecmPrf and the refractivity calculated from radiosonde data, respectively.

AMTD
5, 8405–8434, 2012

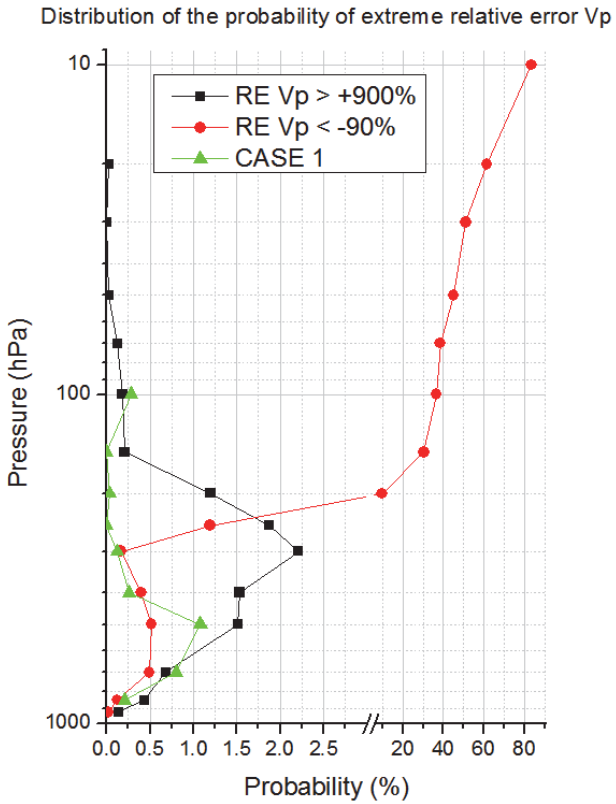

Fig. 7. Distribution of extreme relative error of water vapor pressure. The black curve shows the probability of data whose relative error of water vapor pressure larger than +900 %, the red curve shows the probability of data whose relative error of water vapor pressure smaller than −90 % The green curve shows the probability of case 1 described in the paper.

AMTD
5, 8405–8434, 2012

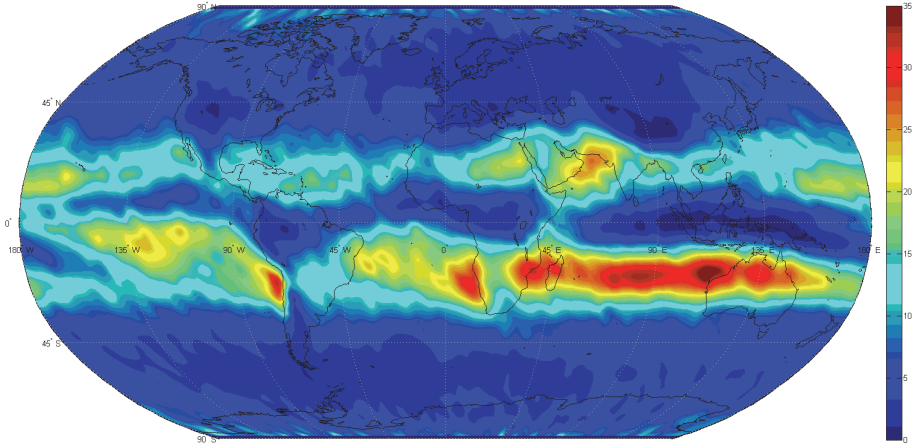

Fig. 8. Distribution of the probability of the profiles which contains extremely small humidity data($Vp < 2 \times 10^{-6}$ hPa) The grid is 5° × 5°.

AMTD
5, 8405–8434, 2012

COSMIC radio occultation retrieval product using global radiosonde data

B.-R. Wang et al.

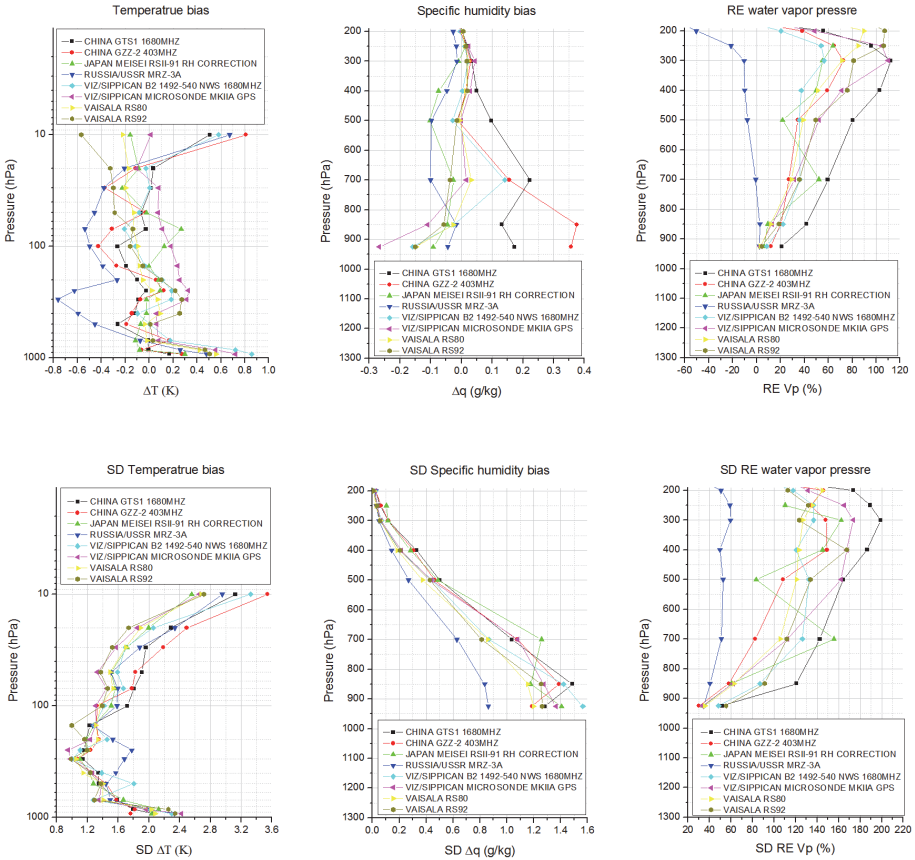

Fig. 9. Differences in mean temperature bias, mean specific humidity bias, relative error of water vapor pressure and their SDs between COSMIC and different radiosonde types. Radiosonde data is the benchmark (Eqs. 7–9).

AMTD
5, 8405–8434, 2012

COSMIC radio occultation retrieval product using global radiosonde data

B.-R. Wang et al.

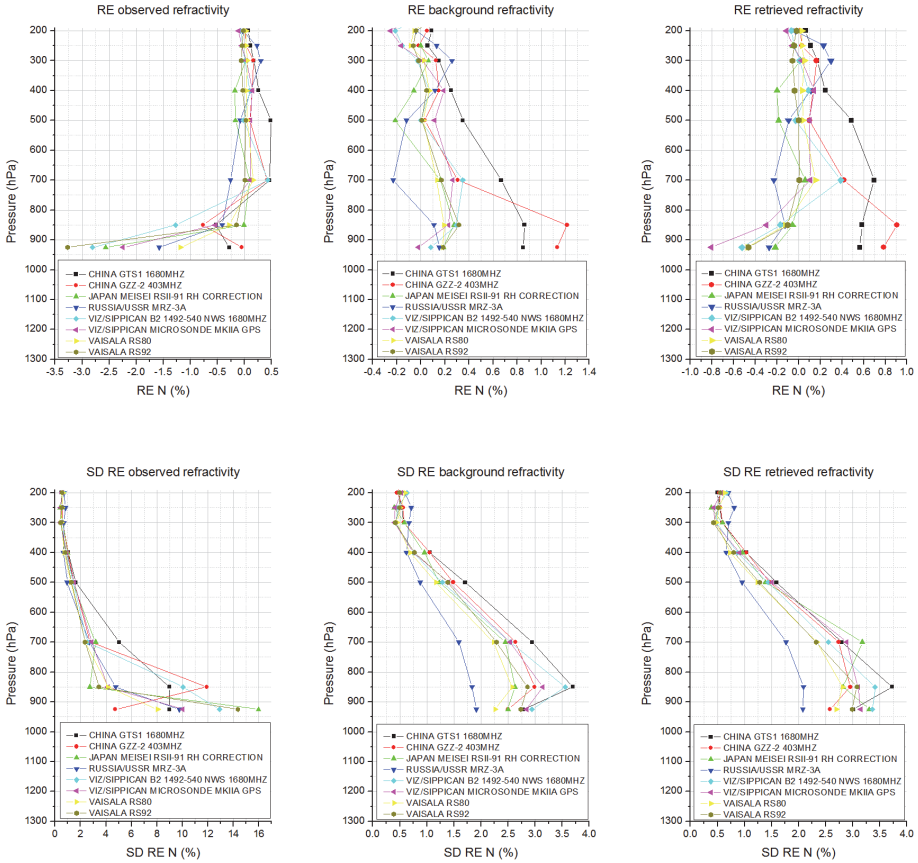

Fig. 10. Relative error and SD between the refractivity of different radiosonde types and the refractivity from the 1DVAR product wetPrf, radio occultation observation, and background, respectively (Eq. 10).

AMTD
5, 8405–8434, 2012

COSMIC radio occultation retrieval product using global radiosonde data

B.-R. Wang et al.